

UC Berkeley

UC Berkeley Previously Published Works

Title

Carbon isotope fractionation by an ancestral rubisco suggests that biological proxies for CO₂ through geologic time should be reevaluated

Permalink

<https://escholarship.org/uc/item/8mw4m0q1>

Journal

Proceedings of the National Academy of Sciences of the United States of America, 120(20)

ISSN

0027-8424

Authors

Wang, Renée Z
Nichols, Robert J
Liu, Albert K
[et al.](#)

Publication Date

2023-05-16

DOI

10.1073/pnas.2300466120

Copyright Information

This work is made available under the terms of a Creative Commons Attribution-NonCommercial-NoDerivatives License, available at <https://creativecommons.org/licenses/by-nc-nd/4.0/>

Peer reviewed



Carbon isotope fractionation by an ancestral rubisco suggests that biological proxies for CO₂ through geologic time should be reevaluated

Renée Z. Wang^{a1} , Robert J. Nichols^b, Albert K. Liu^{cd} , Avi I. Flamholz^e , Juliana Artier^f , Doug M. Banda^g , David F. Savage^{bh} , John M. Eiler^a, Patrick M. Shih^{cf}, and Woodward W. Fischer^a

Edited by François Morel, Princeton University, Princeton, NJ; received January 11, 2023; accepted April 14, 2023

The history of Earth's carbon cycle reflects trends in atmospheric composition convolved with the evolution of photosynthesis. Fortunately, key parts of the carbon cycle have been recorded in the carbon isotope ratios of sedimentary rocks. The dominant model used to interpret this record as a proxy for ancient atmospheric CO₂ is based on carbon isotope fractionations of modern photoautotrophs, and longstanding questions remain about how their evolution might have impacted the record. Therefore, we measured both biomass (ϵ_p) and enzymatic ($\epsilon_{\text{Rubisco}}$) carbon isotope fractionations of a cyanobacterial strain (*Synechococcus elongatus* PCC 7942) solely expressing a putative ancestral Form 1B rubisco dating to $\gg 1$ Ga. This strain, nicknamed ANC, grows in ambient pCO₂ and displays larger ϵ_p values than WT, despite having a much smaller $\epsilon_{\text{Rubisco}}$ ($17.23 \pm 0.61\%$ vs. $25.18 \pm 0.31\%$, respectively). Surprisingly, ANC ϵ_p exceeded ANC $\epsilon_{\text{Rubisco}}$ in all conditions tested, contradicting prevailing models of cyanobacterial carbon isotope fractionation. Such models can be rectified by introducing additional isotopic fractionation associated with powered inorganic carbon uptake mechanisms present in Cyanobacteria, but this amendment hinders the ability to accurately estimate historical pCO₂ from geological data. Understanding the evolution of rubisco and the CO₂ concentrating mechanism is therefore critical for interpreting the carbon isotope record, and fluctuations in the record may reflect the evolving efficiency of carbon fixing metabolisms in addition to changes in atmospheric CO₂.

evolution | carbon isotopes | rubisco | cyanobacteria | Precambrian

Photoautotrophs have evolved over geologic time to harness energy from the sun in order to “fix” external, inorganic carbon (C_i) into reduced, organic carbon (C_o), thereby creating biomass for growth and energy storage. Today, and likely for much of Earth's history (1), the most widespread strategy for carbon fixation is the Calvin–Benson–Bassham (CBB) cycle, where the key carbon fixation step is catalyzed by ribulose-1,5-bisphosphate (RuBP) carboxylase/oxygenase (rubisco) (2, 3). But rubisco's central role in the CBB cycle and oxygenic photosynthesis poses a conundrum because it is usually considered to be a non-specific and slow enzyme. The first issue concerns rubisco's dual carboxylase and oxygenase activities: The RuBP intermediate (enediolate) is susceptible to both O₂ and CO₂ attacks (4). Consequently, instead of fixing a CO₂ molecule during photosynthesis, rubisco can instead assimilate O₂ to yield 2-phosphoglycolate (2-PG), which is not part of the CBB cycle and therefore must be salvaged through photorespiratory pathways that consume adenosine triphosphate (ATP), reducing power, and carbon (5). The second issue concerns rubisco's maximum carboxylation rate (V_c), which is ≈ 7 to 10 times slower than other central metabolic enzymes (6), and displays very limited variation across large phylogenetic distances (7).

Both issues—its dual carboxylase/oxygenase activity and limited maximum carboxylation rate—are typically rationalized by considering its evolutionary history in the context of long-term changes in environmental CO₂ and O₂ concentrations. Rubisco is thought to have been the primary carboxylating enzyme of global photosynthesis since the Great Oxygenation Event and potentially far prior (1). It is also thought to have evolved when there was trace O₂ and much higher CO₂ concentrations in the atmosphere, in contrast to the modern atmosphere where O₂ is roughly 20% while CO₂ is only about 0.04% by partial pressure (1).

Likely in response to these changing environmental concentrations, many aquatic photoautotrophs evolved CO₂ concentrating mechanisms (CCMs) that enhance carboxylation and suppress oxygenation by immersing rubisco in a high-CO₂ environment. Even with CCMs, the effective in vivo rates of extant rubiscos are estimated to be lower ($\approx 1\%$ for

Significance

Earth scientists rely on chemical fossils like the carbon isotope record to derive ancient atmospheric CO₂ concentrations, but interpretation of this record is calibrated using modern organisms. We tested this assumption by measuring the carbon isotope fractionation of a reconstructed ancestral rubisco enzyme (>1 billion years old) in vivo and in vitro. Our results contradicted prevailing models of carbon flow in Cyanobacteria, but our data could be rationalized if light-driven uptake of CO₂ is considered. Our study suggests that the carbon isotope record tracks both the evolution of photosynthetic physiology as well as changes in atmospheric CO₂, highlighting the importance of considering both evolution and physiology for comparative biological approaches to understanding Earth's history.

Author contributions: R.Z.W., R.J.N., A.K.L., D.F.S., J.M.E., P.M.S., and W.W.F. designed research; R.Z.W., R.J.N., A.K.L., J.A., and D.M.B. performed research; R.Z.W., R.J.N., A.K.L., A.I.F., and J.A. analyzed data; D.F.S., J.M.E., P.M.S., and W.W.F. advised on project; and R.Z.W. and A.I.F. wrote the paper.

The authors declare no competing interest.

This article is a PNAS Direct Submission.

Copyright © 2023 the Author(s). Published by PNAS. This open access article is distributed under [Creative Commons Attribution-NonCommercial-NoDerivatives License 4.0 \(CC BY-NC-ND\)](https://creativecommons.org/licenses/by-nc-nd/4.0/).

¹To whom correspondence may be addressed. Email: rzwang@caltech.edu.

This article contains supporting information online at <https://www.pnas.org/lookup/suppl/doi:10.1073/pnas.2300466120/-/DCSupplemental>.

Published May 8, 2023.

terrestrial and $\approx 15\%$ for marine rubiscos) than the maximal catalytic rates measured at 25°C (2). Today, all known Cyanobacteria have CCMs, as do many bacterial chemolithoautotrophs, many aquatic algae and some plants (8). The bacterial CCM has two main components: i) C_i pumps producing high cytosolic HCO_3^- concentrations, and ii) coencapsulation of carbonic anhydrase (CA) and rubisco inside proteinaceous organelles known as carboxysomes (Fig. 1A) (9–11). These C_i pumps include BCT1 (ATP-dependent powered HCO_3^- transporter), SbtA ($\text{Na}^+/\text{HCO}_3^-$ symporters), BicA (Na -dependent HCO_3^- transporter), NDH-1MS, and NDH-1MS' (NADPH-dependent powered CO_2 uptake; see ref. 12 for review). It is unclear exactly when the bacterial CCM arose, with proposals ranging from the Proterozoic to the Phanerozoic Eon (8, 13). Therefore, for up to half of Earth's history, cyanobacterial rubiscos have functioned in concert with a system that pumps C_i into and around the cell.

Rubisco displays a kinetic isotope effect (KIE) where it preferentially fixes $^{12}\text{CO}_2$ over $^{13}\text{CO}_2$ due in part to the V_C being slightly faster for $^{12}\text{CO}_2$ than $^{13}\text{CO}_2$ (21), leading the reaction product, 3-phosphoglycerate (3-PG), to be relatively depleted in ^{13}C by several percent (tens of ‰) relative to the isotopic composition of the CO_2 substrate. This effect is typically reported in delta ($\delta^{13}\text{C}$) and epsilon (ϵ) notation in units of per mille (‰), where $\delta^{13}\text{C} = [^{13}\text{R}_{\text{sa}}/^{13}\text{R}_{\text{ref}} - 1] \times 1000$ and ^{13}R is the ratio of $^{13}\text{C}/^{12}\text{C}$ in the sample or reference, respectively; see *Materials and Methods*. The difference in $\delta^{13}\text{C}$ of the CO_2 substrate and the 3-PG product is reported as $\epsilon_{\text{Rubisco}}$ and varies between 18 and 30‰ for extant rubiscos (22, 23), with the exception of the coccolithophore *E. huxleyi* with $\epsilon_{\text{Rubisco}} \approx 11\%$ (24). Because autotrophs utilizing the CBB cycle synthesize biomass from 3-PG, biomass is ^{13}C -depleted compared to external C_i pools—the magnitude of this difference is called ϵ_p .

The KIE of rubisco, along with other and more minor processes that affect carbon isotope ratios, is recorded in the carbon isotope record, which is comprised of measurements of the relative ratios of ^{13}C to ^{12}C isotopes in C-bearing phases of sedimentary rocks

over time (25). Carbon isotope data have been assembled globally from myriad of ancient environments to cover ≈ 3.8 billion years (Ga) of Earth's 4.5 Ga history (26). Contemporaneous C_i pools are preserved as carbonate salts (e.g., limestones and dolomites), while contemporaneous biomass and C_o pools are preserved in the organic-rich components (e.g., kerogen) of many different lithologies and are measured as rock total organic carbon (TOC) (25). There are additional fractionations associated with the preservation of biomass and C_i as rocks, so the magnitude of fractionation between rock C_i and C_o is termed ϵ_{TOC} and differs slightly from ϵ_p (27). Therefore, if one can derive ϵ_p from the rock record (ϵ_{TOC}) and pair it with a model relating ϵ_p to $p\text{CO}_2$, in principle one can infer the history of atmospheric $p\text{CO}_2$ from the carbon isotope record.

The carbon isotope record is particularly important for constraining ancient atmospheric $p\text{CO}_2$ (28, 29) because direct observations of the past atmosphere from trapped gas in ice cores only extends back ≈ 1 million years (30). One notable feature of the record from ≈ 3.8 Ga to the present is that rock C_o is depleted in ^{13}C by $\approx 25\%$ compared to C_i (23, 25, 26), and this offset roughly matches the KIE of extant rubiscos (25). The dominant model used to derive ancient atmospheric CO_2 from the geological record (referred to as the “C Isotope Record Model” here; *SI Appendix*, Fig. S7 and Eq. 1) reflects this observation by fixing the maximum possible fractionation of biomass to be that of rubisco:

$$\epsilon_p = \epsilon_f - \frac{b}{[\text{CO}_2(\text{aq})]}, \quad [1]$$

where ϵ_f is the maximum isotopic fractionation for carbon fixation and is typically set to equal $\epsilon_{\text{Rubisco}}$, $[\text{CO}_2(\text{aq})]$ is the concentration of dissolved CO_2 in solution around the cells, and b is a fitted parameter derived from experiments (31). This physiological factor, b ($\% \text{ kg } \mu\text{M}^{-1}$), is fit from pure culture experiments of eukaryotic and bacterial algae, and encompasses all physiological effects that may affect cellular isotopic fractionation including the CCM, growth rate, cell size and geometry, membrane permeability,

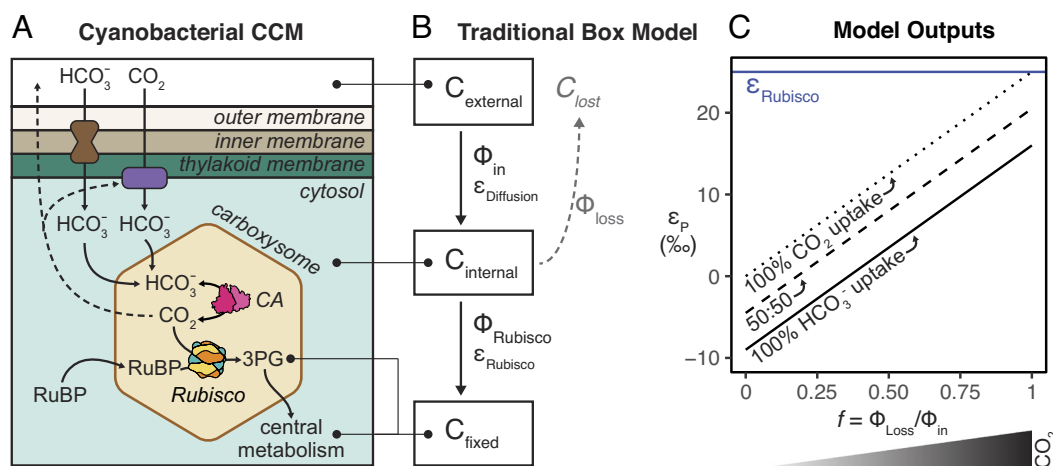


Fig. 1. Comparing the cyanobacterial CO_2 concentrating mechanism (CCM) to the traditional box model of photosynthetic C isotope discrimination. (A) Cyanobacterial CCMs rely on i) active C_i uptake into the cell, and ii) coencapsulation of carbonic anhydrase (CA) and rubisco within the carboxysome. Independent, powered transporters for HCO_3^- and CO_2 are shown in brown and purple; both work to increase cytosolic concentrations of HCO_3^- (see ref. 12 for review). All CCM components work to produce a high carboxysomal CO_2 concentration that enhances CO_2 fixation by rubisco and suppresses oxygenation. Limited CO_2 escapes from the carboxysome—some is scavenged by CO_2 pumps while the rest leaves the cell. (B) Architecture of the traditional box model based on (14–17); see *SI Appendix* for full discussion of this model. Boxes denote carbon pools of interest, and fluxes between boxes are denoted by Φ . Each flux has its own isotopic fractionation denoted by ϵ ; no fractionation is assumed for Φ_{loss} . Model assumes an infinitely large external carbon pool, that carbon not fixed by rubisco (C_{lost}) returns to this pool, and that fluxes are at steady state. Note that this architecture does not include a box for the carboxysome. (C) Model solution for the traditional model is $\epsilon_p = \sigma^* \epsilon_{\text{equil}} + f^* \epsilon_{\text{Rubisco}}$ (Eq. 2), where ϵ_p is defined as the difference in $\delta^{13}\text{C}$ of C_{external} and C_{fixed} , f is defined as the fraction of C_i loss ($\Phi_{\text{loss}}/\Phi_{\text{in}}$), and σ^* is the fractional contribution of HCO_3^- to total C_i uptake. When $\sigma^* = 0$, all C_i uptake is as CO_2 (dotted line); when $\sigma^* = 1$, all C_i uptake is as HCO_3^- (solid line). This model is presented in ref. 18, which is a generalization of (19) that accounts for the fact that C_i uptake (Φ_{in} in Panel B) ranges in composition between CO_2 and HCO_3^- based on which C_i uptake system is used. Values of $\epsilon_{\text{Rubisco}} = 25\%$ and $\epsilon_{\text{equil}} = -9\%$ were used for this illustration (20). Model outputs indicate that at high external CO_2 concentrations (dark wedge under graph), there is greater net C_i leakage (larger f values) from the cell.

growth medium composition (e.g., pH, salinity, limiting nutrient), strain genetics, and physiological state (31–35). In the limit of high $[\text{CO}_2(\text{aq})]$, the term $b/[\text{CO}_2(\text{aq})]$ goes to zero and $\epsilon_p = \epsilon_f$, which is assumed to equal $\epsilon_{\text{Rubisco}}$. Therefore, with this model framework the maximum value of ϵ_p is $\epsilon_{\text{Rubisco}}$, and the term b sets how quickly ϵ_p approaches the limit of $\epsilon_{\text{Rubisco}}$.

The term b and the assumption that $\epsilon_{\text{Rubisco}}$ sets the upper limit of ϵ_p directly follows from the “traditional model” (Fig. 1 *B* and *C* and Eq. 2) that was developed by measuring ϵ_p of plants and algae while parameters like $p\text{CO}_2$ were varied:

$$\epsilon_p = f * \epsilon_{\text{Rubisco}} + a * \epsilon_{\text{equil}}, \quad [2]$$

where f is a ratio describing how much C_i exits vs. enters the organism ($f = 1$ is all C_i that enters is lost), ϵ_{equil} is the equilibrium isotope effect, and a is the fraction of C_i entering the cell as CO_2 ($a = 0$) or HCO_3^- ($a = 1$) (18, 19). The diffusion isotope effect ($\epsilon_{\text{Diffusion}}$) is considered negligible. This model (Fig. 1 *B* and *C* and Eq. 2) is therefore the physiological underpinning Eq. 1 and subsequent interpretations of the C isotope record; both show a limit where the maximum ϵ_p is $\epsilon_{\text{Rubisco}}$.

This traditional model was originally developed from studies of C isotope fractionation in plants (dotted line in Fig. 1 *C*; all C_i uptake is as CO_2 for plants) and was later adapted to eukaryotic and bacterial algae. The primary architecture of the traditional model stems from a seminal study by Park and Epstein (16) who proposed a “two step model” to explain ϵ_p of tomato plants grown in varied CO_2 concentrations and light levels. In this model, carbon can be viewed as residing in one of three pools or “boxes” (Fig. 1 *B*)— C_i outside the cell (C_{ext}), C_i inside the cell (C_{internal}), or C_o as biomass (C_{fixed}). A “leakiness” term, f , is defined as the ratio of fluxes (Φ) of C_i exiting or entering the plant, where all of the C_i that entered the cell is lost when $f = 1$. In this simplified model, ϵ_p is determined by the isotopic effect of two distinct steps: i) the diffusion of CO_2 into the plant [$\epsilon_{\text{Diffusion}}$; $<1\%$ across a diaphragm cell in water at 25 °C (36)]; and ii) the carbon fixation step catalyzed by rubisco ($\epsilon_{\text{Rubisco}}$; ≈ 18 to 30‰). Notably, Park and Epstein proposed that the isotopic fractionations of these two steps are not additive in vivo (i.e., $\epsilon_p \neq \epsilon_{\text{Diffusion}} + \epsilon_{\text{Rubisco}}$) but instead reflects the process by which photosynthesis is limited, either entry of CO_2 into the cell ($\epsilon_p = \epsilon_{\text{Diffusion}}$) or CO_2 fixation by rubisco ($\epsilon_p = \epsilon_{\text{Rubisco}}$) (16).

Solving the traditional model at steady state results in a linear relationship between ϵ_p and f where the minimum and maximum ϵ_p values are $\epsilon_{\text{Diffusion}}$ and $\epsilon_{\text{Rubisco}}$, respectively (Fig. 1 *C*). This allows experimentally measured values of ϵ_p to be used to solve for CO_2 leakage (f ; Fig. 1 *C*). When $\epsilon_p \approx \epsilon_{\text{Diffusion}}$, nearly all carbon entering the cell is used ($f \approx 0$) and rubisco’s ^{12}C preference is not “expressed”; conversely, when $\epsilon_p \approx \epsilon_{\text{Rubisco}}$, very little of the carbon entering the cell is fixed ($f \approx 1$, nearly all carbon leaks from the cell) and rubisco can “choose” between ^{12}C and ^{13}C substrates so that rubisco’s KIE is fully expressed. Farquhar et al. (17) later derived a relationship between ϵ_p and the ratio of external vs. intracellular CO_2 partial pressures, allowing CO_2 concentrations at the site of rubisco to be roughly estimated from ϵ_p . Therefore, given the assumption that C_i is taken up passively, it is possible to derive an increasing relationship between C_{ext} and ϵ_p from this model, where large ϵ_p indicates that high external CO_2 concentrations generate excess CO_2 at rubisco and ultimately cause more CO_2 to leak out of the cell than can be fixed [see *SI Appendix* and (15)].

This model was later adapted to algae to account for CCMs—mainly active uptake of C_i as HCO_3^- and/or CO_2 —and physiological parameters including growth rate and cell geometry (19, 32, 33, 37, 38). These studies grew eukaryotic and bacterial

algae in a range of $p\text{CO}_2$ and culturing conditions to test if the linear relationship between ϵ_p and $p\text{CO}_2$ observed in plants still held. Interestingly, cyanobacterial ϵ_p was found to be roughly constant independent of environmental $p\text{CO}_2$ and growth rate (32). Because cyanobacterial ϵ_p values were less than known corresponding $\epsilon_{\text{Rubisco}}$ values, additional isotopic fractionation factors were not needed to explain ϵ_p , even though some active C_i transport processes, which may fractionate carbon isotopes, were known in cyanobacteria at the time (39–41). Therefore, though different versions of this “traditional model” exist, all variations essentially modified the plant model by shifting the y-intercept of Fig. 1 *C* to account for uptake of HCO_3^- in addition to CO_2 . If C_i entering the cell is primarily CO_2 , the model effectively represents plants (dotted line in Fig. 1 *C*). If C_i is taken up primarily as HCO_3^- , as in many algae, ϵ_p is shifted to lower values (solid line in Fig. 1 *C*) because of the equilibrium isotopic effect (ϵ_{equil}) between CO_2 and HCO_3^- [$\approx -9\%$ (20)]. In Fig. 1 *C*, we plot the traditional model as derived in Eichner et al. (18), which is an adaptation of (19).

The C Isotope Record Model (Eq. 1 and *SI Appendix*, Fig. S7) and the traditional model (Eq. 2 and Fig. 1 *C*) have a limit where ϵ_p cannot exceed $\epsilon_{\text{Rubisco}}$. Yet, the largest ϵ_p values observed in the Archaean Eon exceed 30‰ (25, 26) and also exceed all current measurements of $\epsilon_{\text{Rubisco}}$ (23). In addition, recent studies in dinoflagellates have shown that ϵ_p can regularly exceed $\epsilon_{\text{Rubisco}}$ under certain growth conditions (22), and detailed studies of Cyanobacteria imply that leakage estimates derived from ϵ_p are not physiologically possible (18). These studies motivated updated models of algal carbon isotope fractionation that account for the isotopic fractionations associated with different C_i uptake mechanisms in order to rationalize anomalous ϵ_p values (18, 22).

These experiments made clear that the physiology of algae and Cyanobacteria—e.g., how they take up C_i as CO_2 or HCO_3^- and by which mechanism—affects the C isotopic content of biomass, ϵ_p . Further, these C_i transporters and other integral components of modern CCMs were once absent from ancient autotrophs, who used various forms of rubisco alone to grow in Archaean or Proterozoic atmospheres (42). Efforts to draw inferences about the ancient Earth from the C isotope record must, therefore, include some understanding of the physiology and evolution of CCMs in Cyanobacteria and eukaryotic algae (22, 42, 43). Recent studies have attempted to address this issue by characterizing model organisms that may better resemble an ancestral counterpart, including a cyanobacterial strain lacking a CCM (43), a strain that overexpresses rubisco (44), and a strain expressing an inferred ancestral rubisco dating from ≈ 1 to 3 Ga (45, 46).

Here, we measured the ϵ_p of a control strain of *Synechococcus elongatus* PCC 7942 expressing the wild-type rubisco (NS2-KanR, referred to as “WT” for “wild-type”, see *Materials and Methods*), as well as a strain, nicknamed “ANC” for “ancestral”, engineered to express an inferred ancestral Form 1B enzyme (dating to >1 Ga) as its sole rubisco (47) in varied CO_2 and light conditions. This putative ancestral rubisco was previously purified and its kinetics were characterized in vitro. Its sequence was then inserted into the genome of a modern cyanobacterium, though the genome of the strain in that study contained both extant and ancestral rubisco sequences (47). Here we study a strain where the extant rubisco was fully removed and replaced with the reconstructed ancestor. In contrast to (46), we also measured $\epsilon_{\text{Rubisco}}$ of the present-day and ancestral rubiscos in vitro. We observed that: i) biomass ϵ_p is greater for ANC than WT for all conditions tested, even though ANC $\epsilon_{\text{Rubisco}}$ ($17.23 \pm 0.61\%$) is considerably smaller than WT $\epsilon_{\text{Rubisco}}$ ($25.18 \pm 0.31\%$); ii) ANC ϵ_p increases with light levels

while WT ϵ_p increases with CO_2 ; iii) ANC displays a growth defect at ambient pCO_2 that is rescued at high pCO_2 ; and iv) ANC growth is severely inhibited in high light. Consistent with recent studies of eukaryotic algae (18, 22), ANC ϵ_p exceeding $\epsilon_{\text{Rubisco}}$ in all conditions implies that the traditional box model is incomplete and additional isotope fractionations are needed to rationalize measured ϵ_p . In addition, modulation of ANC ϵ_p with light suggests that some light-powered component of the CCM is responsible for excess fractionation beyond $\epsilon_{\text{Rubisco}}$. We posit that fractionation due to C_i uptake might explain isotopic measurements that deviate from traditional model predictions in both extant and ancient organisms.

Results and Discussion

Ancestral Rubisco Enzyme Fractionates Less Than the Modern Rubisco. We measured the carbon isotope fractionations of WT and ANC rubiscos in vitro using the substrate depletion method (48–51). Note that there exists experimental variation in $\epsilon_{\text{Rubisco}}$ measurements, both within and across studies, and its cause remains uncertain at present [see *SI Appendix, section 4a* and (52)]; so we employed the same general approach as others (the substrate depletion method) to be consistent with prior literature. Previous work on rubisco isotope discrimination predicted that $\epsilon_{\text{Rubisco}}$ should correlate positively with specificity ($S_{\text{C/O}}$), a unitless measure of the relative preference for CO_2 over O_2 (53). We therefore expected ANC and WT $\epsilon_{\text{Rubisco}}$ values to be the same within uncertainty because of their similar $S_{\text{C/O}}$ values (previously measured in ref. 47), but found that the fractionation factor ($\epsilon_{\text{Rubisco}}$) of the ancestral rubisco ($17.23 \pm 0.61\text{‰}$) was about 8‰ lower than that of the extant rubisco ($25.18 \pm 0.31\text{‰}$, Table 1).

Ancestral Rubisco Strain Grows at Ambient CO_2 Concentrations. Working in *S. elongatus* PCC 7942, we produced a mutant strain lacking the native Form 1B rubisco and expressing instead an ancestral Form 1B rubisco produced by computational ancestral sequence reconstruction (47) as its sole rubisco enzyme. We then grew this strain, termed ANC, and a control strain, termed wild-type or “WT” (*Materials and Methods*), in a variety of light and CO_2 levels: i) a reference condition (ambient pCO_2 of 0.04% v/v, standard light flux (120 μE)); ii) high CO_2 (5% pCO_2 , 120 μE); and iii) high light (0.04% pCO_2 , 500 μE). The CO_2 gas at ambient and high CO_2 conditions had $\delta^{13}\text{C}$ values of -12.46‰ and -36.84‰ , respectively.

Remarkably, as in ref. 46, the ANC strain managed to grow in ambient pCO_2 and standard light conditions (Fig. 2), even though the ancestral rubisco has a V_C roughly half that of WT (Table 1). This implies that its rubisco enzyme is properly encapsulated in the carboxysome, since improper carboxysome formation prohibits growth in ambient air (54, 55). Additional characterization of the physiology of the ANC could be valuable, but our inference of proper carboxysome encapsulation is supported by several experiments and analyses as follows. First, electron micrographs of WT and ANC cells grown in ambient CO_2 and light conditions

(*Materials and Methods*) showed multiple carboxysomes per cell in both strains (Fig. 3 and *SI Appendix, Fig. S13*). Rubisco density can be seen within some of the carboxysomes (Fig. 3C). Second, the rubisco amino acid residues necessary for protein interactions mediating β -carboxysome encapsulation were recently identified (56), and the ANC sequence retains fourteen of the sixteen residues involved (*SI Appendix, Tables S8 and S9* and Fig. S14). In addition, WT and ANC strains harvested during exponential growth in the reference condition exhibit similar photosystem stoichiometry, as indicated by absorbance spectra (*SI Appendix, Fig. S15*). Taken together, these data indicated that carboxysomes form in ANC and the ancestral rubisco is encapsulated within these structures.

In addition, the difference in V_C between the ancestral and modern rubiscos was mirrored in the doubling times of WT and ANC strains (Fig. 2B and *SI Appendix, Table S2*), where ANC doubling times were roughly twice that of WT in the reference condition (20.8 ± 1.2 vs. 12.0 ± 1.4 h, respectively). This suggested that ANC’s growth was limited by its ability to fix CO_2 from ambient air. This growth defect was ameliorated by high pCO_2 , where doubling times for both strains were the same within uncertainty (WT 11.8 ± 0.8 h; ANC 12.0 ± 0.6 h). In contrast to WT, elevated CO_2 greatly accelerated the growth of ANC, reducing its doubling time from ≈ 21 to ≈ 12 h (Fig. 2B), supporting our inference that CO_2 availability limits the growth of ANC in ambient air, implicating the CCM in its growth defect. Similar results were found in ref. 46.

We observed the greatest differences in doubling times between ANC and WT when the strains were grown in high light (500 $\mu\text{mol photons m}^{-2} \text{ s}^{-1}$, Fig. 2 and *SI Appendix, Table S2*). In these conditions, WT cultures were a dark, blue-green color typical of healthy cyanobacterial cells while ANC cultures were yellow-green (*SI Appendix, Fig. S11*), suggesting degradation of phycobilisomes via a known starvation pathway to reduce the cell’s capacity for light harvesting and photochemical electron transport (58, 59). Note that this is a very high light intensity for Cyanobacteria and may induce a severe photoinhibitory response (60). We therefore inferred that ANC could not fix CO_2 at a rate matching its light harvesting capability, and hence expressed this regulatory pathway to decrease light harvesting capacity. WT, in contrast, grew rapidly in high light.

The ANC Strain Fractionates More than WT. Counter to expectations based on $\epsilon_{\text{Rubisco}}$ (Table 1), ANC ϵ_p was as large or larger than WT ϵ_p in all conditions tested (Fig. 4). This was consistent with recent results from a similar ancestral mutant, where that mutant’s ϵ_p values exceeded WT in ambient and elevated CO_2 levels (46). In this study, the highest ANC ϵ_p values were observed for cultures grown in high light, where growth was significantly slower than the WT (doubling time ≈ 50 vs. 4 h, respectively, Fig. 3 and *SI Appendix, Table S3*). ANC ϵ_p values were also modulated differently by light and CO_2 compared to WT. Compared to the reference condition, WT ϵ_p values were indifferent to high light and only increased in high CO_2 (Fig. 4A). In contrast, ANC ϵ_p values did not increase in high CO_2 and only

Table 1. Rubisco characteristics

Rubisco	$\epsilon_{\text{Rubisco}}$ (‰)	V_C (s^{-1})	K_C^{Air} (μM)	V_C/K_C^{Air} ($\text{s}^{-1}\text{mM}^{-1}$)	$S_{\text{C/O}}$
Ancestral form 1B	17.23 ± 0.61	4.72 ± 0.14	168.7	28	49.6 ± 1.8
Modern form 1B	$25.18 \pm 0.31^*$	$9.78 \pm 0.48^*$	184.1*	53.1*	$50.3 \pm 2.0^*$

Starred values (*) for the modern Form 1B were measured in rubiscos purified from *Synechococcus* sp. PCC 6301, which has the same small and large subunit (*RbcS RbcL*) sequences as our working WT strain, *Synechococcus* sp. PCC 7942 (47). Kinetic isotope effect ($\epsilon_{\text{Rubisco}}$, avg. \pm SE) was measured in this study using the substrate depletion method (48–51). Carboxylation turnover under substrate-saturated conditions (V_C); Michaelis constant for CO_2 in ambient levels of O_2 (K_C^{Air}); the catalytic efficiency toward CO_2 in ambient air (V_C/K_C^{Air}); and specificity, a unitless measure of the relative preference for CO_2 over O_2 ($S_{\text{C/O}}$) are from ref. 47.

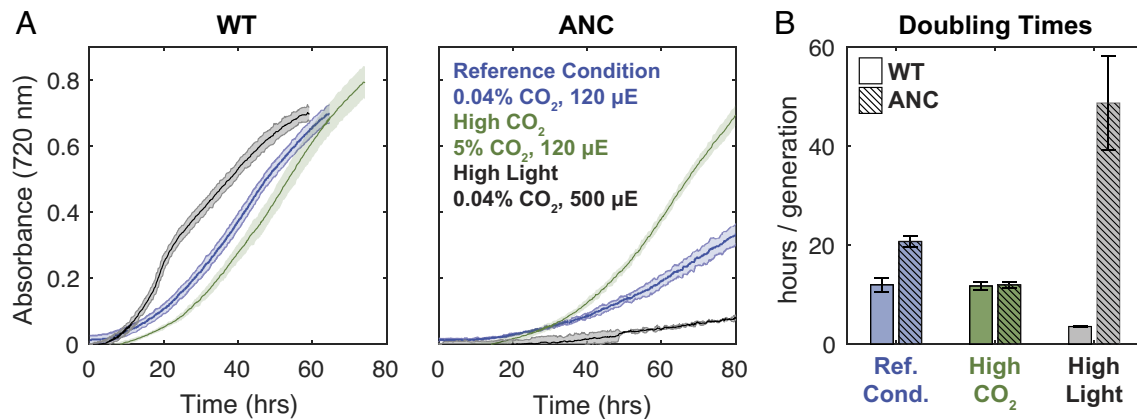


Fig. 2. Growth curves for WT and ANC strains across experimental conditions. (A) Averaged growth curves shown for WT and ANC strains to 80 h, colored by growth condition as indicated in figure. Data were smoothed with a rolling median (*Materials and Methods*); see full ANC growth curves in *SI Appendix, Fig. S12*. (B) Average doubling times with SDs. See *SI Appendix* for details of doubling time calculation. ANC displayed a growth defect relative to the WT at the reference condition, which was rescued by high CO₂. ANC grew slowest in high light, while WT grew fastest in that condition.

increased in high light (Fig. 4B). This result contrasted with the ancestral mutant in ref. 46 where ϵ_p values increased by $\approx 10\%$ at 2% CO₂.

As discussed above, the traditional box model cannot accommodate ϵ_p values in excess of $\epsilon_{\text{Rubisco}}$ (Fig. 1C). However, average ANC ϵ_p values exceeded ANC $\epsilon_{\text{Rubisco}}$ in all growth conditions (Fig. 4), particularly under high-light conditions where the largest difference was seen ($\epsilon_p = 24.30 \pm 0.12\%$ vs. $\epsilon_{\text{Rubisco}} = 17.23 \pm 0.61\%$). The traditional box model also states that ϵ_p values are solely modulated by changing external pCO₂ concentrations, which is plainly contradicted by Fig. 4B.

Proposed Influence of a Light-Powered, Vectoral Carbonic-Anhydrase. Recent studies in extant bacterial and eukaryotic algae have shown that ϵ_p can regularly exceed $\epsilon_{\text{Rubisco}}$ under certain growth conditions (22), motivating updated models of carbon isotope fractionation in both eukaryotic and bacterial algae (18, 22, 61). Taken together, these studies indicated that observed ϵ_p values could only be rationalized if an additional fractionation factor was present. Several studies argued that this factor is an energy-coupled CA catalyzing the vectoral hydration of intracellular CO₂ to HCO₃⁻, as this reaction is calculated to have a large isotopic effect and would allow ϵ_p to exceed $\epsilon_{\text{Rubisco}}$ (18, 22, 61). Energy-coupled CAs can facilitate CO₂ uptake by converting extracellular CO₂ that passively translocates the membrane to intracellular HCO₃⁻ (Fig. 1A), which is advantageous in acidic conditions where CO₂ is the dominant form of extracellular C_i (10, 62, 63).

Vectoral CAs are also thought to potentially “recycle” CO₂ that leaks from the carboxysome by converting it to HCO₃⁻ (12).

Cyanobacteria and eukaryotic algae have two general modes of active C_i uptake: uptake of hydrated C_i (predominantly H₂CO₃ and HCO₃⁻) and of CO₂ (63). In order for the CCM to function, either mode must produce a high, nonequilibrium concentration of HCO₃⁻ in the cytoplasm (8, 10). This is thought to be achieved by coupling CA to an energy source (e.g., light or an ion gradient) that drives the vectoral hydration of CO₂ to HCO₃⁻ in the cytoplasm (64). There is now excellent data supporting this hypothesis in Cyanobacteria, where accessory proteins that bind to the NDH complex, the cyanobacterial homolog of the respiratory Complex I NADH-dehydrogenase, are known to mediate CO₂ uptake specifically (65–67). Additionally, one of these accessory proteins, CupA/B, is reminiscent of a CA and contains a telltale zinc active site situated near a proton channel in a membrane subunit (68). The prevailing understanding of these data is, therefore, that these complexes couple C_i uptake to energy supplied by photochemical electron transport (68, 69). Moreover, a similar protein complex has been described in proteobacterial chemoautotrophs, suggesting that energy-coupled CO₂ hydration is widespread (62).

A vectoral CA would affect ϵ_p for two reasons. First, CO₂ and HCO₃⁻ are isotopically distinct. At equilibrium in standard conditions, HCO₃⁻ is $\approx 9\%$ more enriched in ¹³C than CO₂ (20, 70, 71). Therefore, if a cyanobacterium is predominantly taking up CO₂, the internal C_i pool from which biomass is formed would be isotopically lighter (¹³C-depleted) than if HCO₃⁻ is the

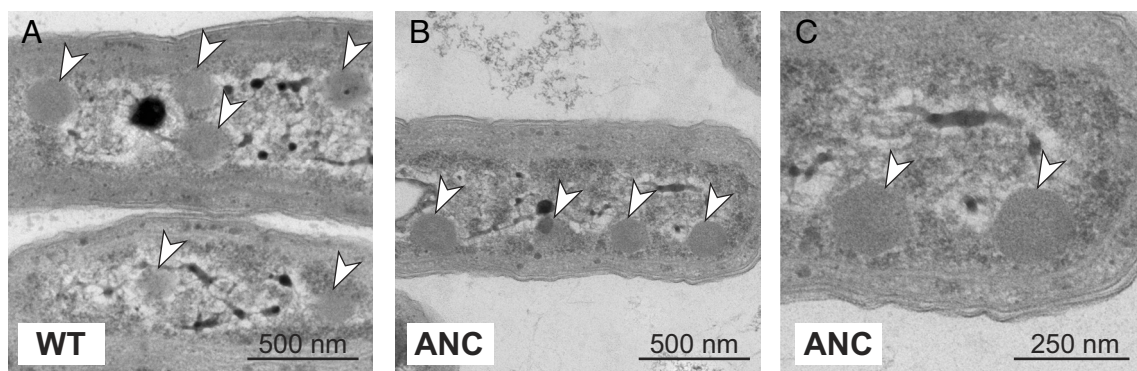


Fig. 3. WT and ANC strains both produce carboxysomes at ambient pCO₂. Transmission electron micrographs of WT (A) and ANC (B and C) strains that were harvested during exponential growth in the reference condition (ambient pCO₂, standard light flux). Both strains show multiple carboxysomes per cell, as indicated by white arrows, and carboxysomes exhibit the typical hexagonal shape (55). (C) is the same image as in (B) but enlarged to show that rubisco density seen can be within the carboxysomes of ANC. The dark internal body in (A) is likely a polyphosphate body (57). See *SI Appendix, Fig. S13* for additional images.

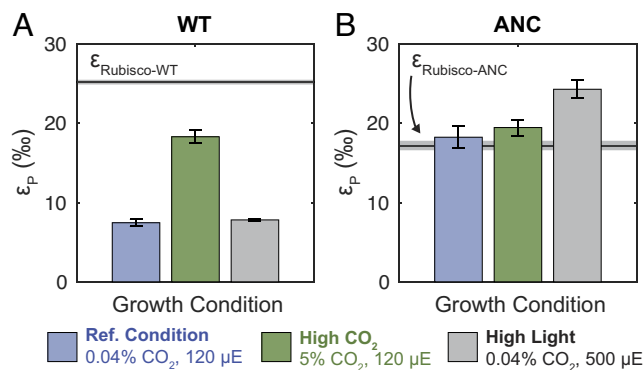


Fig. 4. Whole-cell carbon isotope fractionation by WT and ANC strains. ϵ_p (‰) values (avg. \pm SE) for (A) WT and (B) ANC strains across growth conditions. For each strain, the maximum ϵ_p possible based on the traditional model ($\epsilon_p = \epsilon_{\text{Rubisco}}$) is shown as a gray line (avg. \pm SE). Most measured ANC ϵ_p values exceed the theoretical limit ($\epsilon_p > \epsilon_{\text{Rubisco-ANC}} + \text{SE}$), while WT ϵ_p values do not ($\epsilon_p < \epsilon_{\text{Rubisco-WT}} + \text{SE}$). WT ϵ_p values increase in response to elevated CO₂ concentrations, while ANC ϵ_p values increase in response to elevated light flux. See *SI Appendix, Table S3* for full results.

dominant source of C_i. We focused only on C_i uptake as CO₂ because we were interested in a modification to the traditional model that could achieve large ϵ_p values (indicating ¹³C-depleted biomass) to account for at least an additional ~8‰ of fractionation in ϵ_p (maximum of ~25‰ in the high-light condition) greater than $\epsilon_{\text{Rubisco}}$ (~17‰) in ANC. Though HCO₃⁻ uptake through bicarbonate transporters (e.g., SbtA) was likely occurring under our experimental conditions (65), isotopically it would not help us achieve the measured large ϵ_p values because it would shift all ϵ_p values to be maximally 9‰ more negative (i.e., ¹³C-enriched biomass, Fig. 1C) when we seek to explain values that are ~8‰ more positive. Second, unidirectional CO₂ hydration (CO₂ + H₂O → HCO₃⁻ + H⁺) is expected to impart a substantial KIE, with calculated values ranging from ~19 to 32‰ (70, 72–75). Therefore, there are two mechanistic reasons (CO₂ vs. HCO₃⁻ uptake; unidirectional CO₂ hydration) that ϵ_p could exceed $\epsilon_{\text{Rubisco}}$ in conditions where energized CO₂ uptake and hydration is active. Indeed, a recent model of C-isotope fractionation in Cyanobacteria specifically invoked the NDH complex to rationalize ϵ_p values that exceed $\epsilon_{\text{Rubisco}}$ (18).

Because energy-coupled CO₂ uptake and hydration by the NDH complex is driven by light energy, e.g., via cyclic electron flow around photosystem I (68), and because the vectoral hydration of CO₂ to HCO₃⁻ is thought to have a large carbon isotope fractionation (70, 72–75), ϵ_p should increase with light intensity. Indeed, we observed the largest ANC ϵ_p values in the high-light condition and found that ANC ϵ_p varies primarily with light and not CO₂ (Fig. 4). This observation is counter to the traditional model, which proposes ϵ_p as a direct correlate of external pCO₂ (14, 15). Furthermore, on short timescales (~minutes) cyanobacterial C_i uptake can be modulated by light intensity alone, fully independent of external C_i concentrations (76), and CO₂ uptake can occur in the absence of carbon fixation (77, 78). Based on these physiological and isotopic observations, our study also supports the hypothesis that an energy-coupled vectoral CA like the NDH complex permits $\epsilon_p > \epsilon_{\text{Rubisco}}$, as observed here for ANC in all growth conditions.

Conceptual Model for Carbon Isotope Fractionation in Cyanobacteria. As discussed above, the traditional box model cannot produce $\epsilon_p > \epsilon_{\text{Rubisco}}$ (Fig. 1C). In this model, the C_i leakage term (f) is fit from measured ϵ_p values and $f = 1$ implies that all carbon uptake leaks out of the cell. Though the traditional box

model can accommodate both CO₂ and HCO₃⁻ uptake, which differ in their equilibrium isotopic composition, it does not account for the isotopic effect of vectoral CO₂ hydration. As such, even modeling 100% CO₂ uptake gave physiologically infeasible values of $f > 1$ for ANC in all conditions (Fig. 5A and *SI Appendix, Fig. S8*), yet ANC grew reproducibly in all conditions tested (Fig. 2). We also encountered challenges using the traditional model to rationalize WT data: fitting the model gave $f < 1$ in ambient pCO₂ conditions, but high-CO₂ conditions yielded $f > 1$ unless all C_i uptake was assumed to be as HCO₃⁻ (see *SI Appendix, Fig. S8* for discussion). Therefore, to rationalize our results, we developed a simple modified box model that permits $\epsilon_p > \epsilon_{\text{Rubisco}}$ by including fractionation due to C_i uptake through vectoral CAs.

In this modified model, we explicitly represent the CCM by distinguishing between carbon in the cytosol (C_{int}) and carbon in the carboxysome (C_{carb}), allowing carbon to be lost from the carboxysome (Φ_{Loss2} , Fig. 5B). Therefore, external C_i enters the cell (flux Φ_{in}) where it can either leak out (flux Φ_{Loss1}) or undergo active hydration (flux Φ_{VCA} , where VCA denotes Vectoral CA). Intracellular C_i can then enter the carboxysome, where it is either fixed (flux Φ_{Rubisco}) or ultimately leaks out of the cell (flux Φ_{Loss2}).

We made similar simplifying assumptions as the traditional box model: i) an infinite supply of external carbon, ii) no isotopic fractionation for carbon lost from the cell, iii) Φ_{in} has the isotopic fractionation associated with $\epsilon_{\text{Diffusion}}$, and iv) the system is at steady state. We did not add an explicit term for light energy used to power C_i uptake. Instead, the model included an energized CA (denoted VCA) and its associated isotopic fractionation as free parameters. In modeling each strain, we used the appropriate $\epsilon_{\text{Rubisco}}$ measurements (Table 1). We do not know the true value for ϵ_{VCA} , but used a value of 30‰ similar to a recent model that explicitly invoked the NDH complex in Cyanobacteria (18). For comparison with the traditional model, we plotted Fig. 5C with $f_1 = 0.1$ so that it could be represented in two dimensions; see *SI Appendix, Fig. S10* for full model outputs. In this updated model, each value of ϵ_p corresponds to a set of feasible f_1 and f_2 values that fall along a line (*SI Appendix, Fig. S10*). Therefore, our model constrains but does not uniquely determine f_1 and f_2 , nor does it allow for estimation of external C_i levels because many pairs of f_1 and f_2 values can produce the same ϵ_p .

The modified model was able to rationalize our experimental data of $\epsilon_p > \epsilon_{\text{Rubisco}}$ with leakage values compatible with cell growth ($f_2 < 1$, Fig. 5C). It may also explain why ANC and WT responded so differently to high light. Our model results implied that ANC lost more carbon than WT at the branch point before rubisco (Φ_{Loss2}); i.e., even though carbon was present in the cell, it could not be fixed by the ancestral rubisco, perhaps due to its lower V_C (Table 1). Excess CO₂ allowed rubisco's KIE ($\epsilon_{\text{Rubisco}}$) to be expressed in ϵ_p . These results indicated that, in high light, the vectoral CA was delivering high amounts of CO₂ to both the WT and ANC rubiscos. The faster WT rubisco was able to match this flux, which was reflected in its fast growth rate (Fig. 2) and no change in ϵ_p vs. the reference condition (Fig. 4). However, the slower ANC rubisco was not, which led to its slowest growth rate (Fig. 2), and highest ϵ_p values across all conditions (Fig. 4). Conditions where ϵ_p exceeded $\epsilon_{\text{Rubisco}}$ in ANC suggested that, in addition to Φ_{Loss2} being large (allowing $\epsilon_{\text{Rubisco}}$ to be expressed), Φ_{Loss1} was high as well, which allows ϵ_{VCA} to be expressed. However, since we could not independently determine Φ_{Loss1} and Φ_{Loss2} —i.e., what proportion of ϵ_p reflects the contribution of $\epsilon_{\text{Rubisco}}$ vs. ϵ_{VCA} —we could only conclude that overall the slower ANC rubisco created a “backup” where leakage increased all along the CO₂ fixation pathway and that this effect was exaggerated at high light.

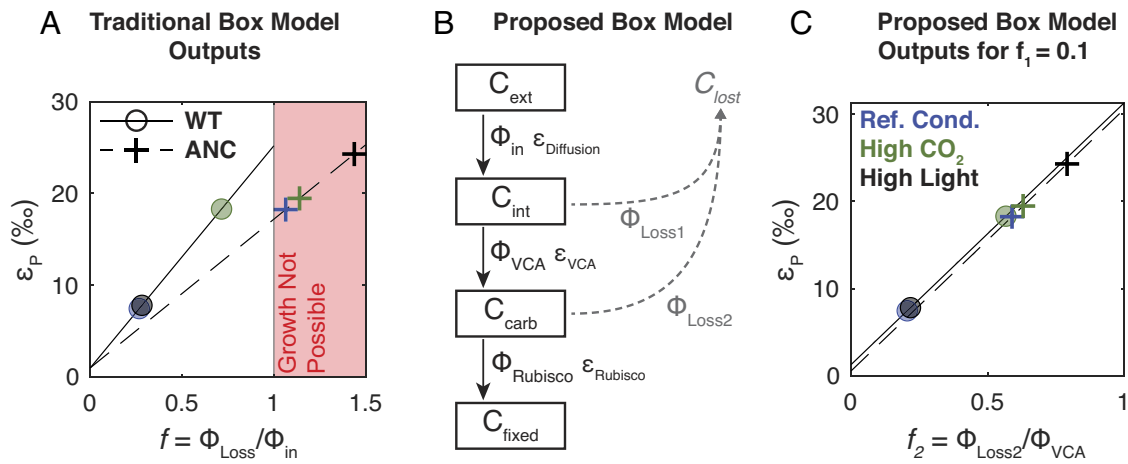


Fig. 5. Proposed box model based on experimental results. (A) Experimental results (circles and crosses) plotted onto traditional box model outputs (solid and dashed lines) for WT and ANC, respectively, if C_i uptake is all CO_2 . See *SI Appendix, Table S11* for quantification of uncertainty. Colors indicate growth conditions as in Fig. 2. The red shaded region demarcates the physiologically infeasible region where $f > 1$. (B) Our proposed box model architecture. Subscripts indicate external (*ext*), internal (*int*), carboxysome (*carb*), and fixed (*fixed*) carbon pools. Fluxes are denoted by Φ where subscripts indicate fluxes into the cell (*in*), out of the cell (*Loss1*, *Loss2*), into the carboxysome (*VCA* for Vectoral Carbonic Anhydrase), and into fixed biomass (*Rubisco*), each with a corresponding isotopic fractionation denoted with ϵ . Loss fluxes were assumed to have no isotopic fractionation. In this model, f_1 is defined as Φ_{Loss1}/Φ_{in} , and f_2 is defined as Φ_{Loss2}/Φ_{VCA} . (C) Experimental results plotted onto proposed box model outputs for $f_1 = 0.1$; colors and symbols are the same as Panel A; see *SI Appendix, Table S11* for quantification of uncertainty. ϵ_p is defined as the difference in $\delta^{13}C$ between C_{ext} and C_{fixed} . Here only results for $f_1 = 0.1$ are shown; see *SI Appendix, Supplementary Text* for full description of model assumptions and results.

We also note that our use of the term “vectoral” CO_2 hydration connotes a net flux that is dominantly in the direction of CO_2 hydration ($CO_2 + H_2O \rightarrow HCO_3^- + H^+$), rather than implying that the flux of HCO_3^- dehydration ($HCO_3^- + H^+ \rightarrow CO_2 + H_2O$) is zero. As such, there is likely some bidirectional activity ($CO_2 + H_2O \rightleftharpoons HCO_3^- + H^+$) of the NDH complex. It is difficult to experimentally measure the isotope effect associated with the CO_2 hydration reaction, but transition state theory and quantum chemical modeling (70, 71, 74) suggest that the value is large (roughly 25‰, see ref. 22 for review). HCO_3^- dehydration, and equilibration in general, would tend to reduce the isotopic fractionation (70). Our results here do not require a larger isotopic effect, however. Rather, a smaller value of $\epsilon_{VCA} = 10\text{‰}$ (*SI Appendix, Fig. S10*) would have allowed us to rationalize our measurements, as we need only account for an additional $\approx 8\text{‰}$ of fractionation in ϵ_p (maximum of $\approx 25\text{‰}$) above $\epsilon_{Rubisco}$ ($\approx 17\text{‰}$) in ANC. See *SI Appendix, Fig. S10* for further discussion.

In addition, ours is not the only model structure that can permit $\epsilon_p > \epsilon_{Rubisco}$. We tested other models by fitting our data to them (*SI Appendix, Fig. S9*). Models that incorporated an explicitly one-way, “CA-like” enzyme (61) or the NDH complex specifically (18) were mostly able to rationalize our data as well. The poorest fits are when C_i uptake was mostly as HCO_3^- (*SI Appendix, Fig. S9*) which is not surprising since we need more positive ϵ_p values and HCO_3^- uptake would shift all ϵ_p values to be 9‰ more negative (Fig. 1C). Altogether, model fitting indicates adding an additional carbon isotope fractionation step produces a model capable of rationalizing our data by enabling $\epsilon_p > \epsilon_{Rubisco}$ with plausible leakage values $f < 1$.

Consequences for Understanding the Evolution of Carbon-Fixing Metabolisms. Our goal was to test if prevailing models of carbon fixation and isotopic fractionation apply to an ancestral analogue strain that may be relevant to understanding the carbon cycle over geologic time. We did so by measuring the isotopic fractionation of a reconstructed ancestral rubisco both inside and outside a living cyanobacterium. We emphasize that ANC is not a true ancestral Cyanobacteria; rather it is a chimeric construct—a modern strain

saddled with a predicted Precambrian enzyme. This reconstructed ancestral rubisco is characterized by slower carboxylation kinetics (47) and a much lower $\epsilon_{Rubisco}$ than the modern strain’s native enzyme ($17.23 \pm 0.61\text{‰}$ vs. $25.18 \pm 0.31\text{‰}$, Table 1).

Recent studies in extant bacterial (18) and eukaryotic algae (22) have motivated updated models of C isotope fractionation in cells; these models address observations that: i) ϵ_p can exceed $\epsilon_{Rubisco}$ in certain conditions; ii) factors other than pCO_2 can modulate ϵ_p . Our results emphasize that similar caveats apply to Cyanobacteria, where ANC ϵ_p exceeded $\epsilon_{Rubisco}$ in all conditions tested. Inference of Archaean and early Proterozoic pCO_2 from the C isotopic record relies intimately on models of cyanobacterial physiology due to their distinction as the oldest oxygenic photoautotrophs (1). Yet, our results show that the traditional form of these models is not generally reliable.

To date, such anomalous ϵ_p values have been observed during relatively slow growth; in ref. 61 $\epsilon_p > \epsilon_{Rubisco}$ occurred early in the growth curve as cells were acclimating to fresh culture media, in ref. 22 $\epsilon_p > \epsilon_{Rubisco}$ occurred during nitrogen and phosphorus limitation, and in this study $\epsilon_p > \epsilon_{Rubisco}$ was observed in a mutant strain growing slowly while expressing a reconstructed ancestral rubisco. These observations indicated that growth physiology affects isotopic fractionation by photosynthetic algae and, in all cases, motivated a rethinking of the traditional box model (Fig. 1 B and C) to include more physiological detail relating to the presence of a CCM.

As high light consistently slowed growth of ANC, induced chlorosis (yellowing of cultures, *SI Appendix, Fig. S11*), and increased ϵ_p , we were motivated to consider the effects of light-related physiology on ϵ_p . The yellowing of ANC cultures in high light was consistent with starvation and taken to indicate that light levels exceeded the downstream capacity for CO_2 fixation (79, 80). We interpreted these observations as indicating that the replacement of the native rubisco with a slower enzyme decreased capacity for CO_2 fixation (Table 1).

Low- CO_2 fixation capacity would not, on its own, explain anomalously high ϵ_p values, however. An additional fractionation process is required to explain ϵ_p values in excess of $\epsilon_{Rubisco}$, which

we assume is due to light-coupled vectorial hydration of CO_2 , which has a large calculated isotope effect (70, 72–75). It is well established that modern Cyanobacteria have light-coupled CO_2 uptake systems (65, 68) and in model Cyanobacteria, this activity is due to the Cup proteins (CupAS/B, also known as Chp proteins), which bind the NDH complex (68, 81). In order for CO_2 uptake to drive the CCM and promote CO_2 fixation, it would need to produce a high, nonequilibrium HCO_3^- concentration in the cytoplasm (8, 10). We and others therefore assumed that the complex of NDH-1 and CupAS/B couples light energy to the vectorial hydration of CO_2 to HCO_3^- at a CA-like active site (68). Disruption of a Cup protein by point mutation was also shown to largely affect cell growth (69), suggesting that the energy-induced directionality is important for Cyanobacteria.

It is apparent from our experiments that $\epsilon_{\text{Rubisco}}$ does not set an upper bound on ϵ_p , nor does it predict which strains will have larger ϵ_p values (Fig. 4). This was only apparent because we measured the isotopic fractionation due to the ancestral rubisco enzyme ($\epsilon_{\text{Rubisco}}$) and compared it to ANC strain biomass (ϵ_p), in contrast with (46), which measured ϵ_p but not $\epsilon_{\text{Rubisco}}$. While our ANC ϵ_p values (≈ 18 to 24‰) fell within the range of ϵ_p values derived from the carbon isotope record (43), they exceeded ANC $\epsilon_{\text{Rubisco}}$ (Fig. 2). Attention has been paid to outliers in the carbon isotope record where ϵ_p exceeds $\epsilon_{\text{Rubisco}}$ precisely because they violate the assumptions underlying the dominant models Eqs. 1 and 2) used to interpret the record (22). In addition, ANC $\epsilon_{\text{Rubisco}}$ ($17.23 \pm 0.61\%$) is anomalously low; not only is it $\approx 8\%$ less than WT $\epsilon_{\text{Rubisco}}$ ($25.18 \pm 0.31\%$) but it is among the lowest measured rubisco KIEs. However, only thirteen unique rubisco KIEs have been measured thus far (23) while ≈ 300 distinct rubiscos have been kinetically characterized (7, 82), suggesting that measuring the isotopic effects of several well-chosen rubisco variants is worthwhile.

Turning to trends in carbon isotope data from the geological record, our results suggested there are at least two nonunique ways to achieve the large ϵ_p values observed earlier in Earth history: i) High external concentrations of C_i , or ii) Active CO_2 uptake driven by photochemical electron transport. Our proposed model (an idealized extension of the traditional model, Eq. 2) cannot be applied readily to the C Isotope Record Model (Eq. 1). Doing so currently gives nonsensical values of b because ANC $\epsilon_p > \epsilon_{\text{Rubisco}}$ (see *SI Appendix, section 6 and Fig. S16* for further discussion), and because we cannot independently constrain the extra degree of freedom introduced (two loss fluxes, Φ_{Loss1} and Φ_{Loss2} , instead of one, f). In addition, these parameters could vary over evolutionary history as the CCM and the efficiency of carbon fixation evolves. Additional measurements that constrain these parameters (i.e., Φ_{Loss1} and Φ_{Loss2}) could enable $p\text{CO}_2$ to be back-calculated from ϵ_p , but further work must be done to then adapt those observations to the C Isotope Record Model (Eq. 2). Importantly, the modified model framework proposed here is not the only approach to producing $\epsilon_p > \epsilon_{\text{Rubisco}}$ with physiologically feasible leakage fluxes. Rather than advocating for our specific model, we offer it as an example form of a solution – showing that ϵ_p can only exceed $\epsilon_{\text{Rubisco}}$ if additional fractionating process is considered. As shown in *SI Appendix, Fig. S9*, several approaches to extending the traditional box model can accommodate $\epsilon_p > \epsilon_{\text{Rubisco}}$ (18, 61), yet all of these models represent substantial simplifications of bacterial and algal CCMs. Overall, our study supports the conclusion of prior studies (18, 22) that a modified traditional model that engages more fully with photosynthetic physiology, like the CCM, is required to more accurately constrain environmental C_i concentrations from ϵ_p .

In addition, this study and other recent work (43, 46) have raised a greater question for the Earth Sciences: What is uniformitarianism for biology? Earth scientists often apply uniformitarian

assumptions—assuming that physical and chemical processes behave the same now as they did billions of years ago—in order to reason about the past. This approach is powerful, but these assumptions are challenged by biological processes that undergo substantial evolution on geologic timescales. Ongoing discoveries of novel metabolisms have supported some principles like “the principle of microbial infallibility”—that microbes will always find a way to take advantage of available energy sources (83)—but it is not clear what principles apply to the details of metabolism. Take rubisco, for example – most extant autotrophs use rubisco to fix carbon, but rubisco sits within a variety of physiologies—e.g., C3, C4, CAM in plants—that temper the effect of $\epsilon_{\text{Rubisco}}$ on ϵ_p (23). We are far from having a clear answer to this question, but recent work at the interface of molecular biology and isotope geochemistry show that these ideas can be tested in the lab. Here and in other recent papers (42, 43, 46), we used synthetic biology to construct organisms with ancestral components so that specific aspects of ancient organisms can be isolated and tested. These “ancestral-like” organisms helped sharpen our understanding of the physiological and environmental factors determining growth (42) and isotopic fractionation (this work) in both ancient and modern autotrophs, showing that models rigidly based on modern taxa are likely not universally applicable across geologic time.

Overall, carbon fixation was a fundamental challenge that autotrophs overcame early in the history of Earth’s biosphere (1). These early processes were recorded in some fashion in the carbon isotope record, but robust interpretation of this record must grapple with the fact that the carbon cycle is an amalgam of both environmental changes and evolutionary processes, mediated by physiology. We now have synthetic biological approaches that offer a way to probe these long timescale coevolutionary problems by producing ancient process analogs of carbon fixation in the laboratory. Utilizing these tools will enable us to better understand how the evolution of key metabolisms have shaped Earth’s chemistry over time.

Materials and Methods

Ancestral Enzyme Reconstruction. Ancestral Rubisco enzyme sequences were previously reported and characterized by Shih et al. (47). Briefly, for both the large subunit and small subunit of Rubisco, encoded by *rbcl* and *rbcS*, respectively, the most recent common ancestor (MRCA) for Form 1A (α), 1B (β), and 1A/B (α/β) clades were predicted from independently derived phylogenetic trees for Rbcl and RbcS containing a broad diversity of Form 1A and 1B Rubisco (>100 sequences). Maximum-likelihood algorithms were used to reconstruct the most probable ancestral sequence for each clade. Ancestral sequences were then expressed in *Escherichia coli* and purified, and enzyme kinetics were measured.

ANC Strain Generation. The “ANC” strain studied here was generated by replacing the native large and small rubisco subunits (*cbbL* and *cbbS*, respectively) of the parent strain (*Synechococcus elongatus* PCC 7942) with the reconstructed β ancestral *cbbL* and *cbbS* sequences. The NS2-KanR (“WT” strain) was generated by inserting a KanR cassette into neutral site 2 (NS2) (GenBank: U44761.1). This was done as a control for having the KanR in the neutral site. *Synechococcus elongatus* PCC 7942 were transformed from the WT strain using the approach of Golden and Sherman (84). Briefly, cultures were grown to OD750 nm = 0.5. Cultures were centrifuged at 18,000 x g for 2 min. Pellets were washed with 100 mM CaCl_2 and spun again at 18,000 x g for 2 min. Pellets were resuspended in BG-11 media followed by addition of plasmid and grown for 16 h in the dark at 30 °C. Transformants were then plated onto BG-11 + KAN100 agar plates and placed under 100 μE of light at 30 °C. Single colonies were selected in media with antibiotic until segregation and then genotyped by PCR amplification of the rubisco locus followed by sequencing to confirm homoplasmic ANC strain rubisco sequence. *SI Appendix, Table S1* lists plasmids and primers used in this study.

Growth Conditions. For ambient CO_2 growth, NS2-KanR (“WT”) and β Ancestral Rubisco-KanR (“ANC”) strains were grown in quadruplicate in a photobioreactor

(Photon Systems Instruments–MC 1000) at the University of California, Berkeley (UC Berkeley) for four biological replicates total. Cultures were grown in buffered BG-11 media with 50mM HEPES at pH 8. Cultures were inoculated at a starting OD720 nm = 0.015 and cultivated at 120 $\mu\text{mol photons m}^{-2} \text{s}^{-1}$, 30 °C, and bubbled with ambient air. High CO₂ growth was performed using the same conditions as ambient growth with the exception of placing the photobioreactor in a 5% CO₂ chamber (Percival AR22L) and bubbling in air from the chamber. High-light growth was performed using the ambient conditions above with the exception of using 500 $\mu\text{mol photons m}^{-2} \text{s}^{-1}$ for light intensity. Cells were harvested by centrifugation at 6000 x g for 20 min at 4 °C. Decanted pellets were then flash frozen with liquid N₂ and lyophilized overnight with the Millrock Technology Model BT85A freeze dryer. Doubling time was calculated by fitting the exponential phase of growth (*k*) using a Markov Chain Monte Carlo (MCMC) approach, using the generic model $y = a \cdot \text{EXP}(k \cdot x) + b$. Growth curves displayed in Fig. 3 were smoothed with a rolling median ($n = 12$) to remove errant readings caused by bubbles advected in front of the detector. See *SI Appendix* for more information.

Carbon Isotope Analysis. Carbon isotope data are reported using delta notation ($\delta^{13}\text{C}$) in units of per mille (‰) where $\delta^{13}\text{C} = \left(\frac{^{13}\text{C}/^{12}\text{C}}{^{13}\text{C}/^{12}\text{C}}_{\text{ref}} - 1 \right) \cdot 1000$, where the subscripts “sa” and “ref” denote sample and reference respectively. The reference used is the Vienna Pee Dee Belemnite (VPDB). $\delta^{13}\text{C}$ values of cyanobacterial cells were measured on an EA-IRMS (Elemental Analyzer Isotope Ratio Mass Spectrometer; Costech Thermo Delta-V) at the California Institute of Technology (Caltech) in Pasadena, CA. Each biological replicate was run four times with two different isotope standards—urea (−27.8‰) and sucrose (−10.45‰). A suite of urea and sucrose standards were run at the beginning, middle, and end of run for sample bracketing and to assess drift throughout the run. An average $\delta^{13}\text{C}$ and SE were calculated and reported for each biological replicate (see *SI Appendix* for more information). The $\delta^{13}\text{C}$ of the starting CO₂ gas was measured on the Thermo Mat 253 Ultra at Caltech; the CALT-2049C standard was used, which has a $\delta^{13}\text{C}_{\text{VPDB}}$ value of −3.62‰. CO₂ gas from high-pCO₂ experiments was sourced from a CO₂ tank, while the CO₂ gas in ambient pCO₂ experiments was distilled from ambient lab air through cryogenic distillation at Caltech. In addition, we labored to keep gas pressures approximately constant during our experiments (i.e., equilibrating to ambient pressure by bubbling) because of potential unwanted isotopic pressure effects. ϵ_p , the carbon isotope fractionation between CO₂ gas and bulk cyanobacterial cells, was calculated as $(\alpha_{\text{CO}_2/\text{bio}} - 1) \cdot 1000$, where $\alpha_{\text{CO}_2/\text{bio}} = \frac{^{13}\text{R}_{\text{CO}_2}}{^{13}\text{R}_{\text{bio}}}$, where ^{13}R is the ratio of ^{13}C to ^{12}C in the analyte. We note this in contrast to other isotope literature where ϵ_p is calculated as $\alpha_{\text{bio}/\text{CO}_2} - 1 \cdot 1000$, which would cause the positive values in this study to be negative. In this study, more positive ϵ_p values indicate more ^{13}C -depleted; see *SI Appendix* for more detail.

Rubisco KIE Assay. *Syn6301* and β -MRCA rubisco were purified according to previous methodologies (85, 86) at University of California, Davis and then shipped on dry ice to Caltech. Clarified lysate from a BL21 DE3 Star *E. coli* culture expressing rubisco was subjected to ammonium sulfate precipitation, at the 30 to 40% cut for *Syn6301* and at the 40 to 50% cut for β -MRCA, followed by anion exchange chromatography and size exclusion chromatography. We then used the substrate depletion method to measure the KIE of the *Syn6301* and β -MRCA rubiscos ($\epsilon_{\text{Rubisco}}$), as used previously in similar studies (48–51). Briefly, an assay mix of HCO₃[−], bovine CA, rubisco, ribulose 1,5-bisphosphate (RuBP), MgCl₂, bicine, and dithiothreitol (DTT) was prepared. As the reaction progressed to completion, aliquots of that assay mix were injected into pre-filled exainers containing phosphoric acid that both stopped the reaction and converted all inorganic carbon species to gaseous CO₂. The $\delta^{13}\text{C}$ of these CO₂ aliquots was then measured on a Delta-V Advantage with Gas Bench and Costech elemental analyzer at Caltech. Here, instead of RuBP being given in excess, CO₂ was given in excess. In addition, instead of determining the fraction of CO₂ (*f*) consumed

independently to create a Rayleigh plot, we fit the curvature of the $\delta^{13}\text{C}$ results to find *f* before converting to a Rayleigh plot to calculate $\epsilon_{\text{Rubisco}}$ similar to previous studies (49). See *SI Appendix* for more information.

Transmission Electron Microscopy Imaging of Whole Cells. WT and ANC strains were grown in the reference condition—buffered BG-11 media, shaking at 250 rpm, with white cool fluorescent light at 120 μE , 30 °C, ambient air (0.04% CO₂ (v/v)). WT and ANC cells were collected at mid-log (40 and 80 h, respectively) at OD730 nm = 0.4 and pelleted by centrifugation (10,000 x g for 10 min). Pelleted cells were then resuspended in 1 mL cold solution 2.5% Glutaraldehyde in 0.1M Sodium Cacodylate Buffer, pH 7.4 (Electron Microscopy Sciences) and stored in the fixative solution at 4 °C until imaging. Sample preparation and sectioning were performed in the Electron Microscope Laboratory core facility at the University of California Berkeley. Briefly, samples were stabilized in 1% low melting-point agarose, cut into small cubes, and then washed at room temperature with 0.1 M sodium cacodylate buffer, pH 7. Samples were then mixed with 1% osmium tetroxide, 1.6% potassium ferricyanide and 0.1 M cacodylate buffer pH 7.2 for an hour in the dark with rotation. These were washed again with a cacodylate buffer pH 7.2, then DI water, and subjected to a 1-h incubation with uranyl acetate 0.5% solution. After a new wash with DI water, samples were dehydrated by an ascending series of acetone concentration (35%, 50%, 75%, 80%, 90%, 100%, 100%). Later, samples were progressively infiltrated in resin (Epon solution: Eponate 12, DDSA NMA and BDMA (Electron Microscopy Sciences) with rotation, followed by a final step at 60°C until polymerized. Thin sections (70 nm) were cut using a Reichert Ultracut E (Leica Microsystems) and collected on 100 mesh formvar-coated copper grids. Sections were poststained using 2% uranyl acetate in 70% methanol and followed with Reynold’s lead citrate. The sections were imaged using a FEI Tecnai 12 transmission electron microscope operated at 120 kV (FEI). Images were collected using UltraScan 1000 digital micrograph software (Gatan Inc).

Data, Materials, and Software Availability. All study data are included in the article and/or *SI Appendix*.

ACKNOWLEDGMENTS. We thank Newton Nguyen for valuable guidance in the MCMC model used to calculate doubling times from growth curve data. We thank Victoria Orphan and Alex Sessions for access to lab space and analytical instruments, as well as lab managers Stephanie A. Connon, Fenfang Wu, and Nami Kitchen for assistance. This research was supported by the David and Lucille Packard Foundation (12540178), Simons Foundation (554187), NASA Exobiology (00010652), and the Schwartz-Reisman Collaborative Science Program (12520057). R.Z.W. was supported by a NSF Graduate Research Fellowship. Work in the lab of D.F.S. was supported by the US Department of Energy (DE-SC00016240). Work in the lab of P.M.S. was supported by a Society in Science-Branco Weiss fellowship from ETH Zürich and a Packard Fellowship from the David Lucille Packard Foundation. We thank Danielle Jorgens and Reena Zalpuri at the University of California Berkeley Electron Microscope Laboratory for advice and assistance in electron microscopy sample preparation and data collection.

Author affiliations: ^aDivision of Geological and Planetary Sciences, California Institute of Technology, Pasadena, CA 91125; ^bDepartment of Molecular and Cell Biology, University of California, Berkeley, Berkeley, CA 94720; ^cPlant Biosystems Design, Lawrence Berkeley National Lab, Joint Bioenergy Institute, Emeryville, CA 94608; ^dBiochemistry, Molecular, Cellular and Developmental Biology Graduate Group, University of California, Davis, CA 95616; ^eDivision of Biology and Biological Engineering, California Institute of Technology, Pasadena, CA 91125; ^fDepartment of Plant and Microbial Biology, University of California, Berkeley, Berkeley, CA 94720; ^gDepartment of Plant Biology, University of California, Davis, CA 95616; and ^hHHMI, University of California, Berkeley, CA 94720

1. W. W. Fischer, J. Hemp, J. E. Johnson, Evolution of oxygenic photosynthesis. *Annu. Rev. Earth Planet. Sci.* **44**, 647–683 (2016).
2. Y. M. Bar-On, R. Milo, The global mass and average rate of rubisco. *Proc. Natl. Acad. Sci. U.S.A.* **116**, 4738–4743 (2019).
3. S. G. Wildman, Along the trail from Fraction I protein to Rubisco (ribulose bisphosphate carboxylase-oxygenase). *Photosyn. Res.* **73**, 243–250 (2002).
4. G. H. Lorimer, T. J. Andrews, Plant photorespiration—an inevitable consequence of the existence of atmospheric oxygen. *Nature* **243**, 359–360 (1973).
5. T. J. Andrews, G. H. Lorimer, *The Biochemistry of Plants: A Comprehensive Treatise, Vol. 10, Photosynthesis*, M. D. Hatch, N. K. Boardman, Eds. (Academic Press, 1987).
6. A. Bar-Even *et al.*, The moderately efficient enzyme: Evolutionary and physicochemical trends shaping enzyme parameters. *Biochemistry* **50**, 4402–4410 (2011).
7. A. I. Flamholz *et al.*, Revisiting trade-offs between rubisco kinetic parameters. *Biochemistry* **58**, 3365–3376 (2019).
8. A. Flamholz, P. M. Shih, Cell biology of photosynthesis over geologic time. *Curr. Biol.* **30**, R490–R494 (2020).
9. B. D. Rae, B. M. Long, M. R. Badger, G. D. Price, Functions, compositions, and evolution of the two types of carboxysomes: Polyhedral microcompartments that facilitate CO₂ fixation in cyanobacteria and some proteobacteria. *Microbiol. Mol. Biol. Rev.* **77**, 357–379 (2013).

10. N. M. Mangan, A. Flammholz, R. D. Hood, R. Milo, D. F. Savage, pH determines the energetic efficiency of the cyanobacterial CO₂ concentrating mechanism. *Proc. Natl. Acad. Sci. U.S.A.* **113**, E5354–E5362 (2016).
11. J. A. Raven, J. Beardall, CO₂ concentrating mechanisms and environmental change. *Aquatic Botany* **118**, 24–37 (2014).
12. G. D. Price *et al.*, The cyanobacterial CCM as a source of genes for improving photosynthetic CO₂ fixation in crop species. *J. Exp. Bot.* **64**, 753–768 (2013).
13. R. Riding, Cyanobacterial calcification, carbon dioxide concentrating mechanisms, and Proterozoic?Cambrian changes in atmospheric composition *Geobiology* **4**, 299–316 (2006).
14. J. M. Hayes, Factors controlling ¹³C contents of sedimentary organic compounds: Principles and evidence. *Mar. Geol.* **113**, 111–125 (1993).
15. R. Francois *et al.*, Changes in the δ¹³C of surface water particulate organic matter across the subtropical convergence in the SW Indian Ocean. *Global Biogeochem. Cycles* **7**, 627–644 (1993).
16. R. Park, S. Epstein, Carbon isotope fractionation during photosynthesis. *Geochim. Cosmochim. Acta* **21**, 110–126 (1960).
17. G. D. Farquhar, M. H. O'Leary, J. A. Berry, On the relationship between carbon isotope discrimination and the intercellular carbon dioxide concentration in leaves. *Aust. J. Plant Physiol.* **9**, 121 (1982).
18. M. Eichner, S. Thoms, S. A. Kranz, B. Rost, Cellular inorganic carbon fluxes in Trichodesmium: A combined approach using measurements and modelling. *J. Exp. Bot.* **66**, 749–759 (2015).
19. T. D. Sharkey, J. A. Berry, "Carbon isotope fractionation of algae as influenced by an inducible CO₂ concentrating mechanism" in *Inorganic Carbon Uptake by Aquatic Photosynthetic Organisms*, W. J. Lucas, J. A. Berry, Eds. (The American Society of Plant Physiologists, 1985), pp. 389–401.
20. W. G. Mook, J. C. Bommerson, W. H. Staverman, Carbon isotope fractionation between dissolved bicarbonate and gaseous carbon dioxide. *Earth Planet. Sci. Lett.* **22**, 169–176 (1974).
21. G. D. Farquhar, A. R. Ehleringer, K. T. Hubick, Carbon isotope discrimination and photosynthesis. *Annu. Rev. Plant Physiol. Plant Mol. Biol.* **40**, 503–537 (1989).
22. E. B. Wilkes, A. Pearson, A general model for carbon isotopes in red-lineage phytoplankton: Interplay between unidirectional processes and fractionation by RubisCO. *Geochim. Cosmochim. Acta* **265**, 163–181 (2019), 10.1016/j.gca.2019.08.043.
23. A. K. Garcia, C. M. Cavanaugh, B. Kacar, The curious consistency of carbon biosignatures over billions of years of Earth-life coevolution. *ISME J.* **15**, 2183–2194 (2021).
24. A. J. Boller, P. J. Thomas, C. M. Cavanaugh, K. M. Scott, Low stable carbon isotope fractionation by coccolithophore RubisCO. *Geochim. Cosmochim. Acta* **75**, 7200–7207 (2011).
25. M. Schidlowski, A 3,800-million-year isotopic record of life from carbon in sedimentary rocks. *Nature* **333**, 313–318 (1988).
26. J. Krissansen-Totton, R. Buick, D. C. Catling, A statistical analysis of the carbon isotope record from the Archean to Phanerozoic and implications for the rise of oxygen. *Am. J. Sci.* **315**, 275–316 (2015).
27. J. M. Hayes, H. Strauss, A. J. Kaufman, The abundance of ¹³C in marine organic matter and isotopic fractionation in the global biogeochemical cycle of carbon during the past 800 Ma. *Chem. Geol.* **161**, 103–125 (1999).
28. J. P. Jasper, J. M. Hayes, A carbon isotope record of CO₂ levels during the late quaternary. *Nature* **347**, 462–464 (1990).
29. M. Pagani *et al.*, The role of carbon dioxide during the onset of Antarctic glaciation. *Science* **334**, 1261–1264 (2011).
30. J. A. Higgins *et al.*, Atmospheric composition 1 million years ago from blue ice in the Allan Hills, Antarctica. *112*, 6887–6891 (2015).
31. R. R. Bidigare *et al.*, Consistent fractionation of ¹³C in nature and in the laboratory: Growth-rate effects in some haptophyte algae. *Global Biogeochem. Cycles* **11**, 279–292 (1997).
32. B. N. Popp *et al.*, Effect of phytoplankton cell geometry on carbon isotopic fractionation. *Geochim. Cosmochim. Acta* **62**, 69–77 (1998).
33. E. A. Laws, B. N. Popp, R. R. Bidigare, M. C. Kennicutt, S. A. Macko, Dependence of phytoplankton carbon isotope composition on growth rate and [CO₂]aq: Theoretical considerations and experimental results. *Geochim. Cosmochim. Acta* **59**, 1131–1138 (1995).
34. Y. G. Zhang, J. Henderiks, X. Liu, Refining the alkenone-pCO₂ method II: Towards resolving the physiological parameter 'b'. *Geochim. Cosmochim. Acta* **281**, 118–134 (2020).
35. G. H. Rau, U. Riebesell, D. Wolf-Gladrow, A model of photosynthetic ¹³C fractionation by marine phytoplankton based on diffusive molecular CO₂ uptake. *Mar. Ecol. Prog. Ser.* **133**, 275–285 (1996).
36. M. H. O'Leary, Measurement of the isotope fractionation associated with diffusion of carbon dioxide in aqueous solution. *J. Phys. Chem.* **88**, 823–825 (1984).
37. N. Cassar, E. A. Laws, B. N. Popp, Carbon isotopic fractionation by the marine diatom *Phaeodactylum tricornutum* under nutrient- and light-limited growth conditions. *Geochim. Cosmochim. Acta* **70**, 5323–5335 (2006).
38. J. A. Berry, "Studies of mechanisms affecting the fractionation of carbon isotopes in photosynthesis" in *Stable Isotopes in Ecological Research, Ecological Studies*, P. W. Rundel, J. R. Ehleringer, K. A. Nagy, Eds. (Springer, New York, 1989), pp. 82–94.
39. H. Gimmler, C. Weiss, M. Baier, W. Hartung, The conductance of the plasmalemma for CO₂. *J. Exp. Bot.* **41**, 785–795 (1990).
40. C. Rotatore, R. R. Lew, B. Colman, Active uptake of CO₂ during photosynthesis in the green alga *Eremosphaera viridis* is mediated by a CO₂-ATPase. *Planta* **188**, 539–545 (1992).
41. D. Sultemeyer, K. Biehler, H. P. Fock, Evidence for the contribution of pseudocyclic photophosphorylation to the energy requirement of the mechanism for concentrating inorganic carbon in *Chlamydomonas*. *Planta* **189**, 235–242 (1993).
42. A. I. Flammholz *et al.*, Trajectories for the evolution of bacterial CO₂-concentrating mechanisms. *Proc. Natl. Acad. Sci. U.S.A.* **119**, e2210539119 (2022).
43. S. J. Hurler, B. A. Wing, C. E. Jasper, N. C. Hill, J. C. Cameron, Carbon isotope evidence for the global physiology of Proterozoic cyanobacteria. *Sci. Adv.* **7**, eabc8998 (2021).
44. A. K. Garcia *et al.*, Effects of RuBisCO and CO₂ concentration on cyanobacterial growth and carbon isotope fractionation. *Geobiology* **21**, 390–403 (2023), 10.1111/gbi.12543.
45. B. Kacar, V. Hanson-Smith, Z. R. Adam, N. Boekelheide, Constraining the timing of the Great Oxidation Event within the RubisCO phylogenetic tree. *Geobiology* **15**, 628–640 (2017).
46. M. Kędzior *et al.*, Resurrected RubisCO suggests uniform carbon isotope signatures over geologic time. *Cell Rep.* **39**, 110726 (2022).
47. P. M. Shih *et al.*, Biochemical characterization of predicted Precambrian RuBisCO. *Nat. Commun.* **7**, 10382 (2016).
48. R. D. Guy, M. L. Fogel, J. A. Berry, Photosynthetic fractionation of the stable isotopes of oxygen and carbon. *Plant Physiol.* **101**, 37–47 (1993).
49. D. B. McNevin, M. R. Badger, H. J. Kane, G. D. Farquhar, Measurement of (carbon) kinetic isotope effect by Rayleigh fractionation using membrane inlet mass spectrometry for CO₂-consuming reactions. *Funct. Plant Biol.* **33**, 1115 (2006).
50. K. M. Scott, J. Schwedock, D. P. Schrag, C. M. Cavanaugh, Influence of form IA RubisCO and environmental dissolved inorganic carbon on the delta ¹³C of the clam-chemoautotroph symbiosis *Solemya velum*. *Environ. Microbiol.* **6**, 1210–1219 (2004).
51. P. J. Thomas *et al.*, Isotope discrimination by form IC RubisCO from *Ralstonia eutropha* and *Rhodospirillum rubrum*, metabolically versatile members of "Proteobacteria" from aquatic and soil habitats. *Environ. Microbiol.* **21**, 72–80 (2019), 10.1111/1462-2920.14423.
52. R. Z. Wang, A. K. Liu, D. M. Banda, W. W. Fischer, P. M. Shih, A bacterial form I' RubisCO has a smaller carbon isotope fractionation than its form I counterpart. *Biomolecules* **13**, 596 (2023).
53. G. G. B. Tcherkez, G. D. Farquhar, T. J. Andrews, Despite slow catalysis and confused substrate specificity, all ribulose biphosphate carboxylases may be nearly perfectly optimized. *Proc. Natl. Acad. Sci. U.S.A.* **103**, 7246–7251 (2006).
54. C. A. Kerfeld, C. Aussignargues, J. Zarzycki, F. Cai, M. Sutter, Bacterial microcompartments. *Nat. Rev. Microbiol.* **16**, 277–290 (2018).
55. G. D. Price, M. R. Badger, Isolation and characterization of high CO₂(2)-requiring mutants of the cyanobacterium *Synechococcus* PCC7942: Two phenotypes that accumulate inorganic carbon but are apparently unable to generate CO₂(2) within the carboxysome. *Plant Physiol.* **91**, 514–525 (1989).
56. H. Wang *et al.*, RubisCO condensate formation by CcmM in β-carboxysome biogenesis. *Nature* **566**, 131–135 (2019).
57. T. E. Jensen, Electron microscopy of polyphosphate bodies in a blue-green alga, *Nostoc pruniforme*. *Archiv. Mikrobiol.* **62**, 144–152 (1968).
58. S. Śliwińska-Wilczewska, Z. Konarzewska, K. Wiśniewska, M. Konik, Photosynthetic pigments changes of three phenotypes of picocyanobacteria *Synechococcus* sp. under different light and temperature conditions. *Cells* **9**, 2030 (2020).
59. T. Grébert *et al.*, Light color acclimation is a key process in the global ocean distribution of *Synechococcus* cyanobacteria. *Proc. Natl. Acad. Sci. U.S.A.* **115**, E2010–E2019 (2018).
60. K. Richardson, J. Beardall, J. A. Raven, Adaptation of unicellular algae to irradiance: An analysis of strategies. *New Phytol.* **93**, 157–191 (1983).
61. J. Erez, A. Bouevitch, A. Kaplan, Carbon isotope fractionation by photosynthetic aquatic microorganisms: Experiments with *Synechococcus* PCC7942, and a simple carbon flux model. *Can. J. Bot.* **76**, 1109–1118 (1998).
62. J. J. Desmarais *et al.*, DABs are inorganic carbon pumps found throughout prokaryotic phyla. *Nat. Microbiol.* **4**, 2204–2215 (2019).
63. T. Ogawa, A. Kaplan, Inorganic carbon acquisition systems in cyanobacteria. *Photosyn. Res.* **77**, 105–115 (2003).
64. M. Volokita, D. Zenvirth, A. Kaplan, L. Reinhold, Nature of the inorganic carbon species actively taken up by the cyanobacterium *Anabaena variabilis*. *Plant Physiol.* **76**, 599–602 (1984).
65. G. D. Price, S. Maeda, T. Omata, M. R. Badger, Modes of active inorganic carbon uptake in the cyanobacterium, *Synechococcus* sp. PCC7942. *Funct. Plant Biol.* **29**, 131 (2002).
66. S. Maeda, M. R. Badger, G. D. Price, Novel gene products associated with NdhD3/D4-containing NDH-1 complexes are involved in photosynthetic CO₂ hydration in the cyanobacterium, *Synechococcus* sp. PCC7942. *Mol. Microbiol.* **43**, 425–435 (2002).
67. B. Klughammer, D. Sultemeyer, M. R. Badger, G. D. Price, The involvement of NAD(P)H dehydrogenase subunits, NdhD3 and NdhF3, in high-affinity CO₂ uptake in *Synechococcus* sp. PCC7002 gives evidence for multiple NDH-1 complexes with specific roles in cyanobacteria. *Mol. Microbiol.* **32**, 1305–1315 (1999).
68. J. M. Schuller *et al.*, Redox-coupled proton pumping drives carbon concentration in the photosynthetic complex I. *Nat. Commun.* **11**, 494 (2020).
69. J. Artier *et al.*, Modeling and mutagenesis of amino acid residues critical for CO₂ hydration by specialized NDH-1 complexes in cyanobacteria. *Biochim. Biophys. Acta Bioenerg.* **1863**, 148503 (2022).
70. Z. Sade, I. Halevy, New constraints on kinetic isotope effects during CO₂(aq) hydration and hydroxylation: Revisiting theoretical and experimental data. *Geochim. Cosmochim. Acta* **214**, 246–265 (2017).
71. R. E. Zeebe, D. Wolf-Gladrow, *CO₂ in Seawater: Equilibrium, Kinetics, Isotopes* (Elsevier, 2001).
72. I. D. Clark, B. Lauriol, Kinetic enrichment of stable isotopes in cryogenic calcites. *Chem. Geol.* **102**, 217–228 (1992).
73. W. Guo, "Carbonate dumped isotope thermometry: Applications to carbonate chondrites and effects of kinetic isotope fractionation", Dissertation (Ph.D.), California Institute of Technology (2009).
74. R. E. Zeebe, Kinetic fractionation of carbon and oxygen isotopes during hydration of carbon dioxide. *Geochim. Cosmochim. Acta* **139**, 540–552 (2014).
75. J. D. Boettger, J. D. Kubicki, Equilibrium and kinetic isotopic fractionation in the CO₂ hydration and hydroxylation reactions: Analysis of the role of hydrogen-bonding via quantum mechanical calculations. *Geochim. Cosmochim. Acta* **292**, 37–63 (2021).
76. D. Tchernov *et al.*, Passive entry of CO₂ and its energy-dependent intracellular conversion to HCO₃⁻ in cyanobacteria are driven by a photosystem I-generated delta muH⁺. *J. Biol. Chem.* **276**, 23450–23455 (2001).
77. G. S. Espie, A. G. Miller, D. T. Canvin, High affinity transport of CO₂(2) in the cyanobacterium *Synechococcus* UTEX 625. *Plant Physiol.* **97**, 943–953 (1991).
78. A. Kaplan, L. Reinhold, CO₂ concentrating mechanisms in photosynthetic microorganisms. *Annu. Rev. Plant Physiol. Plant Mol. Biol.* **50**, 539–570 (1999).
79. J. L. Collier, A. R. Grossman, Chlorosis induced by nutrient deprivation in *Synechococcus* sp. strain PCC 7942: Not all bleaching is the same. *J. Bacteriol.* **174**, 4718–4726 (1992).
80. N. Adir, M. Dines, M. Klartag, A. McGregor, M. Melamed-Frank, "Assembly and disassembly of photobilisomes" in *Complex Intracellular Structures in Prokaryotes, Microbiology Monographs*, J. M. Shively, Ed. (Springer, Berlin Heidelberg, 2006), pp. 47–77.
81. N. Battchikova, M. Eisenhut, E.-M. Aro, Cyanobacterial NDH-1 complexes: Novel insights and remaining puzzles. *Biochim. Biophys. Acta* **1807**, 935–944 (2011).
82. C. Iniguez *et al.*, Evolutionary trends in RuBisCO kinetics and their co-evolution with CO₂ concentrating mechanisms. *Plant J.* **101**, 897–918 (2020).
83. M. A. O'Malley, D. A. Walsh, Rethinking microbial infallibility in the metagenomics era. *FEMS Microbiol. Ecol.* **97**, fiab092 (2021).
84. S. S. Golden, L. A. Sherman, Optimal conditions for genetic transformation of the cyanobacterium *Anacystis nidulans* R2. *J. Bacteriol.* **158**, 36–42 (1984).
85. S. Saschenbrecker *et al.*, Structure and function of RbcX, an assembly chaperone for hexadecameric RubisCO. *Cell* **129**, 1189–1200 (2007).
86. D. M. Banda *et al.*, Novel bacterial clade reveals origin of form I RubisCO. *Nat. Plants* **6**, 1158–1166 (2020).